3D Reconstruction of Reflection Nebulae from a Single Image

Andrei Linţu[1], Lars Hoffmann[2], Marcus Magnor[2], Hendrik P. A. Lensch[1], Hans-Peter Seidel[1]

[1]MPI Informatik, Germany   [2]TU Braunschweig, Germany

Abstract

This paper presents a method for reconstructing the 3D distribution of dust densities in reflection nebulae based on a single input image using an analysis-by-synthesis approach. In a reflection nebula, light is typically emitted from a central star and then scattered and partially absorbed by the nebula's dust particles. We model the light transport in this kind of nebulae by considering absorption and single scattering only. While the core problem of reconstructing an arbitrary 3D volume of dust particles from a 2D image would be ill-posed we demonstrate how the special configuration of light transport paths in reflection nebulae allows us to produce non-exact but plausible 3D volumes. Our reconstruction is driven by an iterative non-linear optimization method, which renders an image in each step with the current estimate of dust densities and then updates the density values to minimize the error to the input image. The recovered volumetric datasets can be used in astrophysical research as well as planetarium visualizations.

1 Introduction

3D models and visualizations of astronomical objects are becoming more and more important nowadays. They are widely used as a tool to prove existing astrophysical theories and to determine various properties of a given astronomical object [6, 15]. They are further used in todays modern planetariums, in which the number of digital video projectors available increased significantly. Realistic 3D flybys of astronomical objects in planetarium shows are becoming rather the rule than the exception. However, most of these animations are created by talented visual artists; in many cases the structure and morphology of the original objects is widely unknown, and therefore the created volume has little in common with astrophysical certainties.

In this paper we address the problem of recon-

Figure 1: The NGC 2023 reflection nebula in Orion which (from [4], courtesy Robert Gendler). The cloud of dust is illuminated by the central star.

structing a plausible 3D volume of a reflection nebula (see Figure 1) using only a single image as input, which can be captured by any telescope. We assume that all light reflected by the nebula originates from a single central star, and that the reflected intensity is due to single scattering and the absorption along the path. Scattering and absorption is correlated to the dust volume density which we aim to reconstruct. Besides the simplified light transport model we do not pose any further restrictions on the nebula, most importantly we do not assume any kind of symmetry as has been formulated in previous reconstruction approaches from single images [12, 10].

Of course, the reconstruction of 3D volumes from 2D images is an under-determined problem. We generate plausible reconstructions by making use of two insights: the intensity of each observed pixel is actually the combined effect of the volume densities along all light paths from the central star towards the viewer. Each voxel of the volume we are reconstructing therefore has a non-local effect on the final image. This implicitly regularizes the

possible solution to some extent. A second result of the specific light transport is that the estimated density for voxels close to the central star have a significant impact on the appearance of a large number of pixels while the area of influence decreases drastically with distance. We account for this effect by optimizing the volume densities in concentric shells, starting with the innermost sphere.

The optimization is driven by an analysis-by-synthesis approach. We make use of a hardware-accelerated volume renderer to determine the appearance given the current estimate of the dust densities. The error to the input image is then minimized based on Powell's algorithm [14]. While we do not claim to correctly reconstruct the original nebula's 3D volume we at least reconstruct a plausible dust distribution that matches the input image. Compared to an initial naive traversal of the volume during optimization, we obtain a better match to the given image and a more plausible 3D volume by following an improved traversal during optimization. Plausible reconstructions can be used for visualization purposes or as starting point for further, more complex physical simulations that incorporate additional measurements.

The structure of the remainder of the paper is as follows: we present related work in the next section. The physics of reflection nebulae and interstellar dust are shortly described in Section 3 and the used lighting model in Section 4. Section 5 presents our reconstruction approach as well as several optimization steps for this specific task. The results of the described reconstruction method are presented in Section 6 and we conclude the paper and present future work in Section 7.

2 Related Work

Recently, there have been large efforts to produce 3D simulations of astronomical nebulae, particularly the Orion nebula [13], where a highly detailed model of the nebula was created, based on data from astrophysical research papers. Time consuming renderings on supercomputers were generated for the final fly-through animation.

There are tomographic reconstruction algorithms that consider scattering in the reconstructed volumes [3] or even diffuse propagation [1]. However, they always build on observations from different projection directions. In our case, due to the large distance to the reflection nebulae only a single projection direction is typically available.

A method for reconstructing the 3D structure of another type of astronomical objects, planetary nebulae, from a single image has been proposed in [12]. The appearance of planetary nebulae is mostly influenced by the self-emission of ionized gas, slightly simplifying the reconstruction problem. Furthermore, the authors apply axial symmetry as a constraint to reduce the complexity of the reconstruction process from 3D to reconstructing a 2D density map, which is rotated around the axis of symmetry to obtain a volumetric dataset. Building on the same idea of axial symmetry the work has been extended to incorporate both emission as well as scattering and absorption found in planetary nebulae with non-negligible dust distributions [10].

In contrast to these methods, our approach is not considering any symmetry in the nebulae to be reconstructed. Instead, we make use of the implicit coupling of volume densities induced by the light transport in reflection nebulae and present an optimization strategy that produces unconstrained, plausible 3D volumes.

For physically-based, realistic volume rendering of synthetic reflection nebula datasets a hardware-accelerated approach has been presented in [11]. The authors of this paper give special attention to the physical correctness of their rendering model. Lacking the availability of real-world 3D volume data sets, the examples presented in the paper are synthetic nebulae which however strongly resemble the possible appearance of real reflection nebulae. We apply and adapt this rendering approach in Section 5.1 to our optimization procedure.

The main contribution of this paper is that we recover a physically plausible 3D volume of an astronomical nebula from a single input image. The obtained datasets can be used as starting approximations by astrophysicists working with 3D models of reflection nebulae as well as for educational purposes in modern day planetarium shows.

3 Reflection Nebula Physics

Reflection nebulae are clouds of dust surrounding one or more young, recently formed stars [2]. The stars in these nebulae are not hot enough to ionize the gas around them but their light is strong enough, so that the reflected light can be observed (see Fig-

ure 1). Their wonderful colors are due to the light of the central star which is scattered and attenuated by the dust surrounding it.

The blue colors seen in these nebulae are mostly due to scattering. This is due to the fact that light at blue wavelengths scatters much more than light at the red end of the visible electromagnetic spectrum. The best example which demonstrates this is the color of the sky; it is blue because it consists of sunlight scattered by the particles in the atmosphere. All reddish colors visible in reflection nebulae account for absorption, the light from the central star gets attenuated and reddened on its way to an observer on earth.

3.1 Interstellar Dust

The physics behind reflection nebulae is actually the physics of the interaction of light with interstellar dust particles. We create a physically-based model of light scattering in interstellar dust using a set of scalar parameters. One is the *albedo* α, which indicates how much light the particles reflect: 0 for total absorption, i.e. black dust, and 1 for the case where all incident light is scattered. In our calculations, we set $\alpha = 0.6$ [5]. In addition, the presence of dust also attenuates any light shining through the dust region, which can be described by an *extinction* parameter τ.

The scattering is further dependent on the angle θ between the incident and the reflected light direction. It is described by the *single particle scattering probability* modeled using the Henyey-Greenstein phase function [7]:

$$\phi(\theta) = \frac{1 - g^2}{2 \cdot (1 + g^2 - 2 \cdot g \cdot \cos\theta)^{3/2}}, \quad (1)$$

where g is an anisotropy factor for forward and backward scattering. Observations and measurements show [5], that equation 1 describes the scattering properties of interstellar dust with a value for $g \approx 0.6$. The effect of varying the anisotropy factor g is described in more detail in [11].

4 Lighting Model

Our volume renderer is based on the following lighting model: the observed radiance $L(x, y)$ at a camera at position c is a function of the aggregated extinction $\tau(v)$, and the albedo $\alpha(v)$ that depend
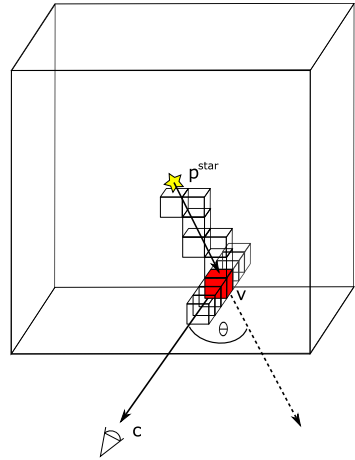

Figure 2: The intensity of the light reflected due to single scattering caused by the red voxel depends on the absorption along the path from the central star to the voxel, the voxel's albedo, the phase function, as wells as on the accumulated absorption along the remaining path towards the viewer.

on the dust density of every voxel v along the ray towards the camera pixel (x, y):

$$L(x, y) = \int_c^\infty e^{-\int_c^v \tau(w)dw} \cdot \alpha(v) \cdot S(v) dv, \quad (2)$$

where $S(v)$ is the total inscattering to the voxel v towards the camera due to the emission L_e^{star} of the nebula's central star(s) at position p^{star}. Considering single scattering only, $S(v)$ is computed as

$$S(v) = \phi(c, v, p^{star}) L_e^{star} \cdot e^{-\int_{p^{star}}^v \tau(w)dw} \quad (3)$$

incorporating the extinction on the way from the star to the voxel as well as the scattering phase function ϕ from the star to the voxel into the direction of the camera c. We assume the same phase function for all voxels. ϕ, L_e^{star}, and p^{star} are assumed to be known. We consider the star to be positioned in the center of the volume. L_e^{star} can be looked up in astrophysical data bases for a specific nebula.

Due to the multiple scattering within a single voxel, the extinction $\tau(v)$ and the albedo $\alpha(v)$ depend non-linearly on the dust density $d_{dust}(v)$. The dust density is the quantity we actually attempt to reconstruct. We precomputed the effective extinction and albedo for a the selected size of a voxel and

all possible dust densities using Monte Carlo simulation, even considering multiple scattering within one voxel. We perform the precomputation for a discrete set of densities spaced $\Delta\varrho$ apart and linearly interpolate for intermediate densities. Our goal is to determine $d_{dust}(v)$ up to a scale factor.

5   3D Reconstruction

Our analysis-by-synthesis approach is driven by the non-linear Powell optimization algorithm [14]. During optimization, we render the current dust density distribution using the equations described in Section 4 and the rendering framework in Section 5.1, and, at every step, we compare the rendering with the given input reflection nebula image.

Before starting the reconstruction process, the input images are cropped to a square and converted to grayscale. One has to make sure that the central star is placed in the center of the image. Since we do not consider self-emission foreground stars are masked out in order to avoid interference with the reconstruction.

The reconstruction process is based on minimizing the following error functional

$$Err = \sum_{x,y=1}^{n} ||L(x,y) - L_{inp}(x,y)||^2 \qquad (4)$$

which is computed using the currently rendered $L(x,y)$ (Equation 2) and the input image L_{inp}.

As can be seen in Figure 2, each voxel has a non-local effect on the rendered image, resulting in some implicit regularization of the optimization. However, this is not constraining the under-determined problem entirely. In the Powell algorithm each voxel is optimized independently. During optimization, the order in which the voxels are processed is very important for the speed and quality of the reconstruction. A naive traversal in a loop over the x, y and z coordinates yields poor reconstruction results, as demonstrated in Figure 3.

The reconstruction artifacts are due to the fact that the radiance reflected by voxels at the outer rim of the volume depends on the dust density values of the inner voxels. During optimization, changes to the inner voxels require updates of the outer voxels which can only be performed after the entire volume has been optimized in one iteration step.

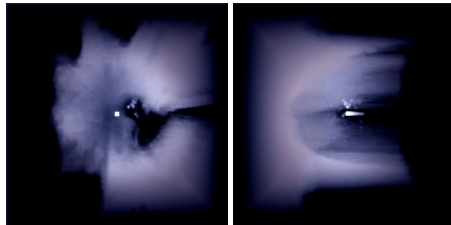We obtain much better results (Figure 5) when the traversal is done starting from the center to the

Figure 3: Inadequate optimization results of NGC 1999 by processing all voxels in scan-line order. Note the decreasing reconstruction quality with increasing distance to the central star. In the side-view (right), an unnatural distribution along the z-axis is visible: the dust is concentrated in the region furthest away from the observer.
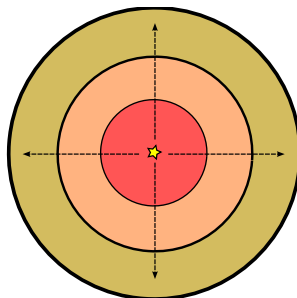

Figure 4: During optimization the volume is traversed starting from the center, in concentric shells.

outside. Voxels closest to the central star are traversed first, resulting in a set of concentric spheres with center at the point of the central star (see Figure 4).

Another observation is that it is better not to start the reconstruction process with an empty volume. It is filled homogeneously with dust densities as small as the smallest $\Delta\varrho$ with which we increment or decrement the voxel dust densities during optimization.

5.1   Rendering and Runtime Optimization

As the lighting calculations are the most computationally expensive, we can obtain a great speedup by accelerating them. We have developed two different options:

To render full frames, and to visualize the results of the reconstruction, we use an OpenGL-based renderer similar to that used for reflection nebulae visualization by Magnor et al. [11]. It is a volume rendering application based on a real time ray-caster implemented on graphics hardware. The implemented algorithm uses the idea described by Krüger et al. [9] to color code the direction of the viewing rays using a bounding box. The algorithm exploits the capabilities of modern graphics hardware to step along the lines of sight querying 3D textures, using a fragment shader to accumulate the inscattering along each ray while considering absorption.

While the hardware-based renderer is significantly faster than a software renderer for computing a full frame, we observe that during the optimization of individual voxels only fractions of the images are actually affected. During optimization, while constantly changing the density of one voxel at a time, only those pixels in the rendered image have to be recomputed which are affected by the new voxel value. The footprint of each voxel is precomputed since it only depends on the ray geometry and is independent on the actual volume density.

A further speed-up as well as an additional means to avoid local minima during the optimization process is achieved by an iterative multi-resolution approach. The reconstruction starts with a lower resolution volume which is scaled up after the end of every iteration. This is done by subdividing each voxel into eight sub-voxels with the same dust density value and applying a 3D Gaussian filter on the dataset for smoothing the resulting high frequencies. We measure a speed-up of factor 2 in the final reconstruction compared to optimizing performed directly at the highest resolution.

6   Results

We present the results of our proposed reconstruction approach for several reflection nebulae: NGC 1999 (Figure 5), the Iris Nebula (Figure 6, top row) and the Cocoon Nebula (Figure 6, bottom row). As already mentioned in section 5, the reconstruction is performed for a grayscale flux image only, speeding up the computation. The here presented results were rendered using spectrally dependent absorption and scattering coefficients. Since our lighting model does not include self-emission we manually removed all stars in the input images since they can-

not be recovered. To produce slightly more realistic final renderings we sometimes added artificial star fields approximating the original image. Reconstruction times for the presented results are between 1-2 days on a 2.4GHz PC with 4GB memory.

For all nebulae we presented the original image, the reconstructed volume rendered from the same view, as well as a rendering of the volume rotated by 90 degrees around the vertical axis. In the frontal views, one can see that the large-scale features are very well reproduced. Some detail has been lost though because the reconstruction has been performed at a maximum resolution of 64^3 voxels. In the bottom right corner of Figure 5, we further present an image of the relative differences between the captured and the reconstructed image, which are overall relatively small. The values are normalized, with 1 corresponding to a difference of 255 in grayscale values.

In the frontal view, the largest error is observed close to the central star. This is because of the lack of self-emission in our framework and can be explained by the algorithm trying to compensate for the high intensity values in the center of the input image (where the central star is situated) by incorrectly adjusting the dust density.

Looking at the side views, one sees a reconstruction that radiometrically agrees with the provided input data, and thus is physically plausible. However, the reconstructed distribution along the z-axis might not necessarily match the expected statistical distribution. It looks slightly too smooth compared to the frontal view. However, it still resembles a reasonable nebula. A good reconstruction is achieved for the Cocoon Nebula (Figure 6, bottom row). We attribute this effect to the slightly less inhomogeneous distribution in the input image. We also have to mention that this nebula has also an emission part, thus not being best suited for reconstruction as a pure reflection nebula.

The most prominent artifacts of our reconstruction are possibly the diagonal features visible in all three side views. While we are not exactly sure, this might be caused by the way how the aggregated extinction $\tau(v)$ and albedo $\alpha(v)$ are precomputed for a single voxel and for every density. During evaluation the voxel is assumed to be perfectly isotropic which of course contradicts the anisotropic shape of a cube, with the largest deviation exactly along the diagonal.
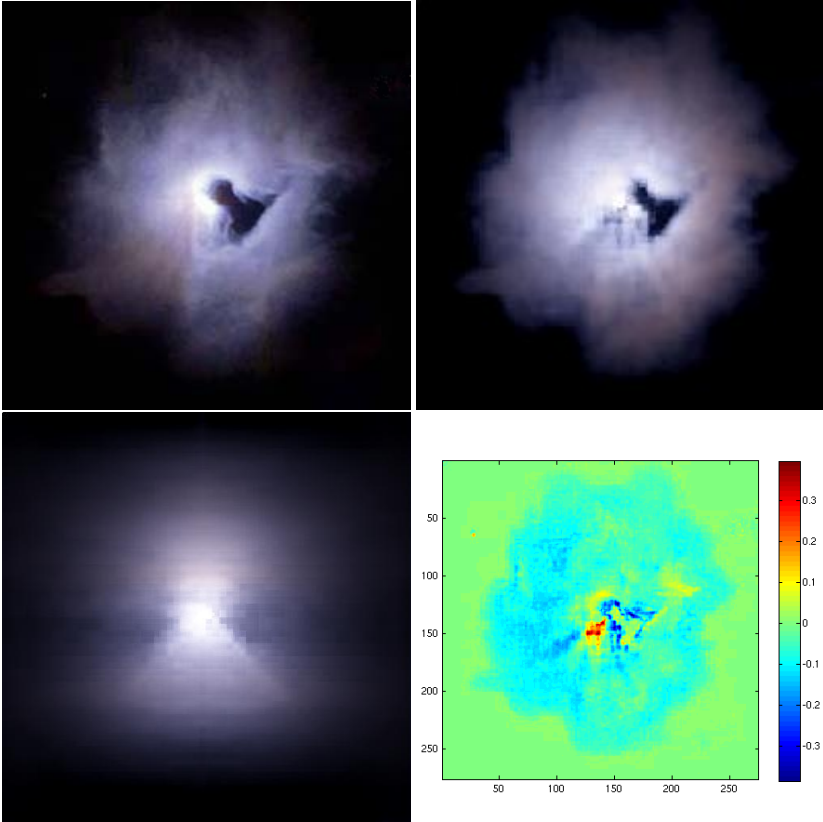
Figure 5: Results for the NGC 1999 nebula. The top row shows the input image (left) and the rendering of the reconstruction from the same viewpoint (right). The bottom row shows a side view of the recovered dust density (left). A color coded difference image between the input image and the rendering of the recovered dust density is presented in the bottom right corner, indicating the good quality of the reconstruction.

In Figure 7, we demonstrate the dependence of the reconstruction results on the intensity of the central stars. We reconstructed the same input image of the nebula NGC 1999 with three different values for L_e^{star}. In order to reproduce the same input pixel intensity, a fainter central star leads to higher dust density values. Conversely, a brighter central star leads to smaller dust density values. With the increasing dust density the different reconstructions also show an increased reddening as explained in Section 3. This effect could actually be used to optimize for the intensity of the central star as well, if wavelength dependent effects are considered during the optimization.

7 Conclusion and Future Work

We presented a reconstruction method for physically plausible volumetric models of reflection nebulae given only single input images. We do not pose any geometric constraints on the shape of the nebulae, such as symmetry which has been applied in previous reconstruction methods. Using an analysis-by-synthesis approach we perform a nonlinear optimization to recover the dust density values. The recovered datasets can later be visualized using a custom renderer and can also be used as starting point for planetarium shows or further physical simulations. While we so far concentrated on the reconstruction of reflection nebulae, it would

Figure 6: From left to right: input image, reconstructed frontal and rendered side view. The top row shows the reconstruction for the Iris Nebula and in the bottom row we present renderings of the Cocoon Nebula. Note, how the structures of the input image are well reproduced in the frontal view. The side views indicated that plausible volumes have been reconstructed.
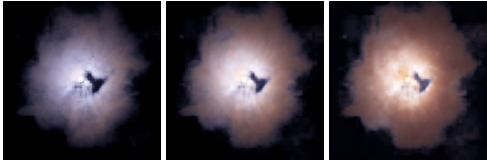

Figure 7: Reconstruction results for different intensity values of the central star, decreasing from left to right. A smaller luminance level leads to higher dust density values and to reddening of the nebula.

be interesting to apply our reconstruction algorithm to other volumetric phenomena that feature single scattering and absorption.

One meaningful extension of our method would be to incorporate multi-wavelength input images; the renderings of the recovered dust density would have to match multiple input images taken with different band filters. Besides the ability of estimating the exact brightness of the central star, as indicated in the previous section, one might be able to obtain a more precise volumetric reconstruction since additional independent constraints are given.

Another promising future research direction would be to add further constraints to the optimization in order to force the statistical distribution of densities along the z-axis to match the statistics of the input image. One could apply for example histogram matching or similar techniques which recently has been successfully applied in the context of solid texture synthesis [8]. Adding such an additional constraint should be rather easy in our current optimization framework.

8 Acknowledgements

References

[1] S. Arridge. Optical tomography in medical imaging. *Inverse Problems*, 15:R41–R93, 1999.

[2] James Binney and Michael Merrifield. *Galactic astronomy*. Galactic astronomy / James Binney and Michael Merrifield. Princeton, NJ : Princeton University Press, 1998. (Princeton series in astrophysics), 1998.

[3] Andrei V. Bronnikov. Numerical solution of the identification problem for the attenuated Radon transform. *Institute of Physics, Electronical Journals*, 1999.

[4] Rob Gendler. The universe in colors. available from `www.robgendlerastropics.com`, 2007.

[5] K. D. Gordon. Interstellar Dust Scattering Properties. In A. N. Witt, G. C. Clayton, and B. T. Draine, editors, *Astrophysics of Dust*, volume 309 of *Astronomical Society of the Pacific Conference Series*, pages 77–+, May 2004.

[6] K. D. Gordon, K. A. Misselt, A. N. Witt, and G. C. Clayton. The DIRTY Model. I. Monte Carlo Radiative Transfer through Dust. *The Astrophysical Journal*, 551:269–276, April 2001.

[7] Louis G. Henyey and Jesse L. Greenstein. Diffuse Radiation in the Galaxy. *Astrophysical Journal*, 93:70–83, 1941.

[8] Johannes Kopf, Chi-Wing Fu, Daniel Cohen-Or, Oliver Deussen, Dani Lischinski, and Tien-Tsin Wong. Solid texture synthesis from 2d exemplars. *ACM Transactions on Graphics (Proceedings of SIGGRAPH 2007)*, 26(3):to appear, 2007.

[9] Jens Krüger and Rüdiger Westermann. Acceleration techniques for GPU-based volume rendering. In Greg Turk, Jarke J. van Wijk, and Robert Moorhead II, editors, *14th IEEE Visualization 2003 Conference (VIS 2003), 19-24 October 2003, Seattle, WA, USA*, pages 287–292. IEEE Computer Society, 2003.

[10] Andrei Linţu, Hendrik P. A. Lensch, Marcus Magnor, Sascha El-Abed, and Hans-Peter Seidel. 3D Reconstruction of Emission and Absorption in Planetary Nebulae. In Hans-Christian Hege and Raghu Machiraju, editors, *IEEE/EG International Symposium on Volume Graphics*, September 2007. to appear.

[11] Marcus Magnor, Kristian Hildebrand, Andrei Linţu, and Andrew J. Hanson. Reflection Nebula Visualization. In C.T. Silva, E. Gröller, and H. Rushmeier, editors, *Proceedings of the IEEE Conference on Visualization (VIS'05)*, pages 255–262, Minneapolis, USA, October 2005. IEEE.

[12] Marcus Magnor, Gordon Kindlmann, Charles Hansen, and Neb Duric. Constrained inverse volume rendering for planetary nebulae. In *Proc. IEEE Visualization 2004, Austin, USA*, pages 83–90, October 2004.

[13] David R. Nadeau, Jon D. Genetti, Steve Napear, Bernard Pailthorpe, Carter Emmart, Erik Wesselak, and Dennis Davidson. Visualizing stars and emission nebulas. *Comput. Graph. Forum*, 20(1):27–33, 2001.

[14] William H. Press, Saul A. Teukolsky, William T. Vetterling, and Brian P. Flannery. *Numerical Recipes in C: The Art of Scientific Computing*. Cambridge University Press, Cambridge, MA, 2. edition, 1992.

[15] K. Wood, J. S. Mathis, and B. Ercolano. A three-dimensional Monte Carlo photoionization code for modelling diffuse ionized gas. *Monthly Notices of the Royal Astronomical Society*, 348:1337–1347, March 2004.